Influence of anisotropy and walls thickness on the mechanical behavior of 3D printed onyx parts

Daouda Nikiema, Pascale Balland, Alain Sergent

CIRP Journal of Manufacturing Science and Technology 50 (2024) 185–197

Contents lists available at ScienceDirect

CIRP Journal of Manufacturing Science and Technology

journal homepage: www.elsevier.com/locate/cirpj

Influence of anisotropy and walls thickness on the mechanical behavior of 3D printed onyx parts

Daouda Nikiema *, Pascale Balland, Alain Sergent

Université Savoie Mont Blanc, SYMME, F-74000 Annecy, France

ARTICLE INFO

Keywords:
3D printing
Effect of walls
Orientation and positioning
Mechanical characterization
Numerical simulation

ABSTRACT

Predicting the behavior and mechanical properties of 3D-printed parts is crucial for 3D printer users. This study conducted experimental investigations on Onyx 3D-printed parts to identify the most important printing parameters. These parameters were specimen positioning and the number of specimen walls. The experimental results indicated that specimens oriented in the XZ direction were 48% stiffer than those oriented in the XY direction and 54% stiffer than those oriented in the ZX direction. Additionally, the results demonstrated that walls significantly influenced the mechanical properties of specimens in the XY and XZ orientations but had no effect on those in the ZX orientation. The Young's modulus increased by 60% between a specimen with one wall and another with eight walls. This paper presents an analytical model for predicting mechanical properties based on the number of walls, with a prediction error ranging from 1% to 15%. Additionally, a numerical simulation approach was proposed to predict the mechanical behavior of parts. The numerical and experimental results comparison showed a 1% to 9% prediction error and a good correlation between numerical and experimental curves. These findings can be a valuable aid to engineers in the design of 3D printed mechanical concepts.

1. Introduction

Recent advancements in additive manufacturing (AM) processes have led to their adoption in various industrial sectors, including medical, automotive, defense, and aerospace. This technology generates significant revenue. For example, according to a 2022 report by Wohlers Associates, the revenue generated from the commercialization of polymer-based powder bed fusion reached $900 million in 2021, which is expected to continue growing in the coming years [1]. The progress in AM technologies has also facilitated the development of efficient processes to meet industrial requirements, such as new 3D printers capable of printing short or long fiber-reinforced composites [2]. Like any manufacturing process, the characterization of the process and the mechanical properties of the obtained parts are crucial steps before scaling up the use of AM on a larger scale. Numerous research studies have been conducted on various AM processes, including 3D printing or fused deposition modeling (FDM). For instance, Patel et al. [3] reviewed the parameters for 3D printing composites, while Prabahkar et al. [4] identified key printing parameters that can influence the mechanical and geometric properties of printed parts. These parameters include the material type, nozzle temperature, layer thickness, layer printing angle, pattern type, pattern density, and printing speed.

The mechanical characterization of parts produced by 3D printing has been investigated in several studies. Chacón et al. [5] demonstrated that the studied material, polylactic acid (PLA), exhibits anisotropic mechanical behavior, meaning its behavior depends on the printing direction. Zou et al. [6] found that an isotropic behavior can be observed in acrylonitrile butadiene (ABS) when printing parameters are neglected. Marşavina et al. [7] studied the impact of printing parameters on the tensile and fracture properties of PLA specimens. The study revealed that specimen orientation and layer thickness were the parameters that influenced these properties. The authors also observed that the presence of walls in the specimens ensured good mechanical properties, particularly fracture toughness. However, when these parameters are considered, anisotropic behavior must be considered. Recently, Liu et al. [8] showed that the energy absorption capacity strongly depends on the pattern used, printing direction, and number of walls. They identified that a triangular pattern, a flat printing direction, and two walls were optimal parameters for achieving optimal energy absorption. In contrast, Gebisa et al. conducted two separate studies [9,10] and demonstrated that walls contribute less to the increase in tensile and flexural properties than other parameters, such as angle and lattice

* Correspondence to: 5 Chemin de Bellevue, 74944 Annecy-Le-Vieux Cedex, France.
E-mail addresses: daoudanikiema94@gmail.com, daouda.nikiema@univ-smb.fr (D. Nikiema).

https://doi.org/10.1016/j.cirpj.2024.03.002
Received 29 June 2023; Received in revised form 27 January 2024; Accepted 7 March 2024
Available online 12 March 2024

width. Távara et al. [11] reported a difference in mechanical behavior depending on the orientation angle of 3D printed Onyx samples. In particular, they showed that specimens with layers oriented at 0°/90° were stiffer than those with layers oriented at + 45°/− 45° and also observed different fracture surfaces between the samples. They concluded their work by recommending the use of anisotropic mechanical behavior when defining the overall mechanical behavior of Onyx. Khosravani et al. [12] demonstrated that the printing direction of layers affects the Young's modulus and mode I fracture toughness of ABS printed parts. They also improved the surface roughness of the parts by treating them with acetone. However, this treatment reduced the mechanical strength of the parts. In reference [13], it was shown that 3D-printed ABS parts exhibit significant anisotropy in their fracture behavior, which is attributed to the printing direction of the layers. Therefore, it is crucial to consider this factor when designing 3D-printed parts. Adibeig et al. [14] recently demonstrated that printing direction and layer orientation can simultaneously induce anisotropic mechanical behavior in 3D-printed parts made of carbon-fiber-reinforced ABS. These studies demonstrate that printing parameters significantly impact the mechanical properties of printed parts. Analytical and numerical prediction tools can aid in designing 3D-printed parts due to the numerous printing parameters involved.

Predicting mechanical properties and performing a numerical simulation of 3D-printed parts have garnered scientific attention. Lupone et al. [15] proposed analytical models for predicting the mechanical properties of carbon fiber-reinforced 3D-printed parts. Melanka et al. [16] also employed analytical models to predict the mechanical properties of 3D-printed parts reinforced with long fibers. The Rule of Mixtures (ROM) is one of the most commonly used analytical models in the literature [17,18] for predicting mechanical properties. Regarding numerical simulation, the adopted mechanical behavior models are generally isotropic. For example, Ripalla et al. [19] employed an isotropic behavior model in their numerical simulations. Domingo-Espin et al. [20] used an orthotropic behavior model in their simulations, and nine parameters were identified through tensile testing. Khosravani et al. [21] conducted numerical simulations of the fracture of PLA-printed parts. They experimentally determined the influence of printing angles on the specimens and found anisotropic behavior. Based on their results, they proposed an anisotropic mechanical behavior model to simulate the fracture behavior of the parts. The simulation results showed good agreement with the experimental behavior. The studies have not adequately addressed a key parameter of 3D printing: the effect of walls, both experimentally and numerically. Ignoring this parameter makes it impossible to predict the behavior and mechanical properties of 3D-printed parts adequately. In addition, there has not been a thorough investigation of Onyx, a primary material for printing functional parts.

To address the limitations of previous research, this study conducted experimental and numerical investigations to propose an approach for predicting the mechanical properties of 3D printed Onyx parts by considering the influence of walls and positioning of parts on the printing platform. This will provide engineers with a valuable tool for predicting mechanical properties as a breakthrough in 3D printing. When designing for 3D printing or other manufacturing processes, it is necessary to use numerical or analytical prediction tools. These tools enable designers to reduce the number of physical tests, reducing design costs. This is the motivation for the present work. The manuscript has been organized into four sections to carry out this work. The first section presents the experimental approach, where the fabrication of the test specimens, printing parameters, and the experimental test are described. The second section presents both the experimental results and the analytical prediction methodology that was developed. The third section proposes numerical simulation approaches for 3D-printed parts, considering the key parameters identified. Finally, the last section presents the conclusions of the work and outlines future investigations.

2. Experimental method

The experimental approach employed in this section involves conducting tensile tests on specimens to determine the influence of positioning, orientation, and walls on the mechanical properties of printed parts. An overview of the printer and the studied specimens was provided to achieve this. Subsequently, a method for characterizing specimens without walls and with walls only was also presented. Finally, a tomographic study of the cross-sections of the different specimens was conducted.

2.1. 3D Printer, samples fabrication, and mechanical testing

The Markforged X7 printer was used in this work. It is equipped with two print heads, allowing for the printing of parts reinforced with long fibers or parts without reinforcement. The parts studied in this work are without reinforcement, meaning they were printed using only plastic. Onyx is the base plastic material used in this printer. According to the manufacturer, it consists primarily of a blend of nylon (polyamide 6) and approximately 10 to 20% by volume of micro carbon fibers. In [22], details of Onyx composition can be found in the image obtained by scanning electron microscopy. The reinforcement options available for this machine include glass fibers, Kevlar fibers, and carbon fibers.

The studied specimens have a rectangular cross-section, with the shape and dimensions obtained from the ASTM D3039 standard (Fig. 1). The CAD model of the specimen was designed using SolidWorks software (professional version) and exported to the printer's slicer software (Eiger) in STL format (Standard Tessellation Language). The slicer software is where the printing parameters are set, and the printed parts are shown in Fig. 2(a). In most tests conducted, the fracture zone of the test specimens was observed within the useful length of the specimens, specifically between the extensometer knives, as shown in Fig. 2(b). This indicates that the shape, specimen dimensions and test conditions were correctly chosen. The mechanical properties of these analyses were as realistic as possible for the material studied.

The mechanical tests conducted in this study were exclusively uniaxial tensile tests, following the recommendations of the ASTM D638 standard. The Instron 5569 universal testing machine with a 50 kN load cell and a 12.5 mm gauge length extensometer was used. The test speed was set at 10 mm/min. The mechanical properties analyzed include Young's modulus, yield strength, and ultimate tensile strength. To calculate the Young's modulus, the linear part of the stress-strain curve was considered using linear regression in Excel, as was also done by Hasanov et al. [23]. The validity criterion was a regression coefficient $R^2 > 0.99$. Each specimen was printed in triplicate and tested under identical conditions to ensure accuracy. The elastic limit adopted is $Re_{0.2}$, which corresponds to the elastic limit at 0.2% plastic strain, similar to the approach taken by Narajo-Lozada et al. [24]. Ultimate tensile strength was the maximum mechanical stress of the stress-strain curve.

2.2. Study of the mechanical behavior of Onyx

The investigation of mechanical properties in this section aims to determine the anisotropy of the printed parts using the Markforged X7 printer. This study focuses on the orientation and positioning of the parts on the print bed. The printing parameters used in this study are presented in Table 1.

2.2.1. Orientation of the parts on the printing platform

The orientation of the parts on the printing platform was investigated. This involved printing the specimens at different angles on the printer's build platform and testing and evaluating this orientation's influence on the mechanical properties. The angles studied were 0°, 45°, 90°, and 135°, respectively (as shown in Fig. 3).

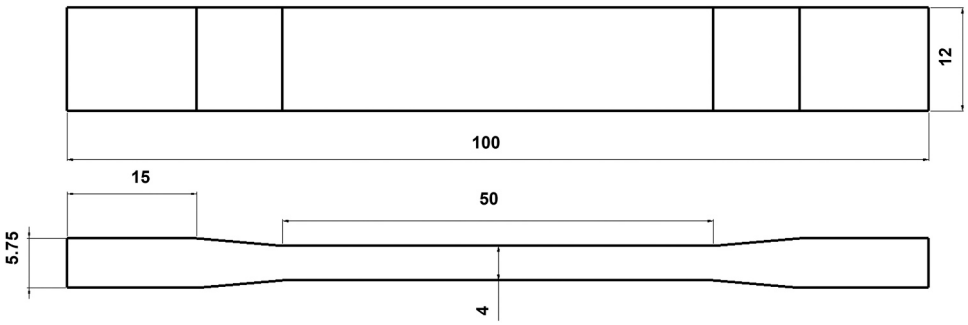

Fig. 1. Specimen geometry and dimensions in millimeters.

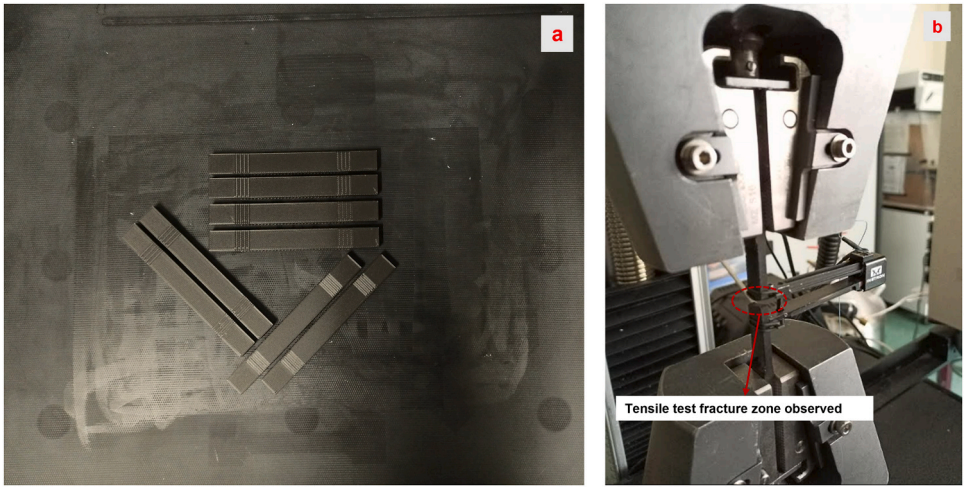

Fig. 2. (a) printed parts and (b) tensile test of samples.

Table 1
Printing parameters.

Printing parameters	Specifications
Pattern - density	Solid – 100%
Layer thickness – wall width (mm)	0.1 – 0.4
Part orientation angle (°)	0, 45, 90 and 135
Part positioning	XY, XZ, and ZX
Wall (contours) count	2 to 8
Deposition angle of successive (°)	±45
Nozzle temperature (°C)	273

2.2.2. *Positioning of the parts on the printing platform*

This work identified and studied three main positioning configurations on the print bed. The different positions are flat (XY), lateral (XZ), and vertical (ZX), as shown in Fig. 4. The objective of this investigation is, first, to characterize the difference in mechanical behavior among these three positionings and, second, to determine the anisotropy coefficient of the process. Eq. 1 was used to calculate the anisotropy coefficient, and it was developed as a result of the work of Ye et al. [25] and Dey et al. [26].

$$I_{3D} = \sqrt{(f_{XY} - f_{filament})^2 + (f_{XZ} - f_{filament})^2 + \frac{(f_{ZX} - f_{filament})^2}{f_{filament}}} \quad (1)$$

Where f_{XY}, f_{XZ}, f_{ZX} and $f_{filament}$ are mechanical parameters of XY, XZ, ZX samples and Onyx filament, respectively. These parameters can be the Young's modulus (E), yield strength (Re) or maximum strength (Rm) of the parts. In this study, the parameter used is Young's modulus. The value of the anisotropy coefficient (I_{3D}) is always positive and greater than or equal to 0. When the coefficient value is close to or equal to 0, it indicates that the process is isotropic or quasi-isotropic and that its influence on the mechanical properties is negligible. However, when the coefficient is high, the process induces an anisotropy in the mechanical properties.

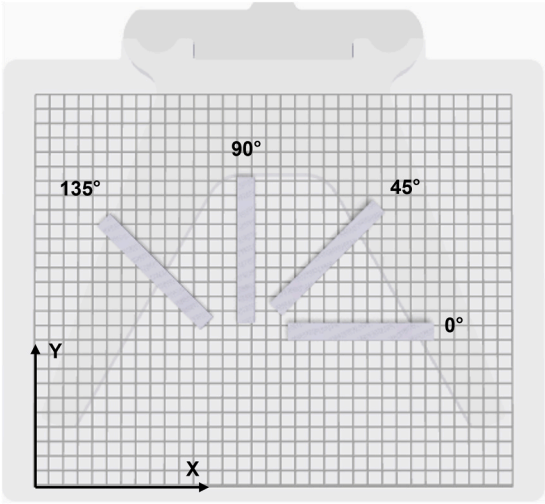

Fig. 3. Parts orientation on the printing platform.

2.3. *Influence of walls*

The influence of walls was characterized by varying the number of

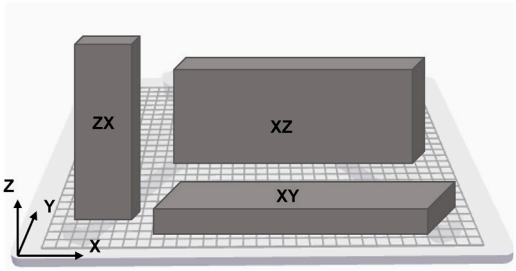

Fig. 4. Parts positioning on the printing platform.

walls (contours) on the test specimens. The investigations were performed on the three positionings (XY, XZ, and ZX) of the specimens. Table 2 summarizes the number of walls used for each positioning type.

A specimen with five walls was printed to characterize the walls alone, and then the walls were isolated by cutting to be characterized separately. To characterize the solid pattern alone, specimens with one wall were printed, and the same cutting method was used to remove the walls and obtain specimens without walls (consisting only of the solid pattern), which were then characterized. An illustration of the different numbers of walls is presented in Fig. 5.

3. Experimental results and prediction of mechanical properties

3.1. Influence of orientation on mechanical properties

The average mechanical properties of the specimens according to the orientation angle on the printing platform are presented in Table 3. Results show that the mean values of the Young's modulus (E_{mean}) do not vary significantly, with a variation between 2306 and 2544 MPa, corresponding to a variation of about ± 3.5% around the mean modulus of all specimens. Similar observations were made regarding the average values of the yield strength (Re_{mean}) and the maximum strength (Rm_{mean}), with variations ranging from 26–30 MPa and 42–48 MPa, respectively. The supplier provided a Young's modulus value of 2400 MPa, consistent with the average values obtained in this study. Based on these results, and without considering the influence of positioning, Onyx can be considered an isotropic material. This finding aligns with previous studies, such as those by Žmindák et al. [27] and Kalova et al. [28], which also considered Onyx to be isotropic in numerical simulation models. Benamira et al. [29] demonstrated that the mechanical properties of PLA-printed parts are not influenced by orientation.

The stress-strain curves (shown in Fig. 6) revealed that the specimens oriented at 0° and 90° are 65% more ductile than those oriented at 45° and 135°. The orientation of successive printing layers relative to the direction of tension may explain this change in behavior. For example, the 0°-oriented specimens have their layers oriented at ± 45° with respect to the direction of tension. In comparison, the 45°- or 135°-oriented specimens have their successive layers oriented at 0° and 90° with respect to the printing direction. In the work of Ságа et al. [30], the results showed that the specimen with layers oriented at 0°/90° has a 48% higher Young's modulus than the one with layers oriented at ± 45°. Távara et al. [11] demonstrated that specimens with layers at + 45° and − 45° (equivalent to the 0° specimen in this study) undergo more deformation than specimens with layers at 0° and 90° (equivalent to the 45° specimen in this study).

Table 2
Number of walls studied for each type of positioning.

	XY	XZ	ZX
Number of walls	1-2-4-8	1-2-3	1-2-3

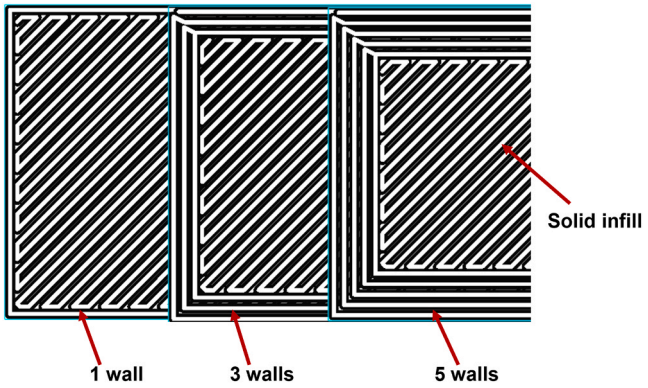

Fig. 5. Illustration of the number of walls.

Table 3
Mechanical properties according to the different angles (average values and standard deviation).

	E_{mean}	Re_{mean}	Rm_{mean}
	(MPa)	(MPa)	(MPa)
0°	2437 ± 105	30 ± 3	48 ± 0.9
45°	2382 ± 22	26 ± 1	42 ± 0.5
90°	2306 ± 64	29 ± 1	48 ± 1
135°	2544 ± 74	27 ± 0.5	45 ± 0.5

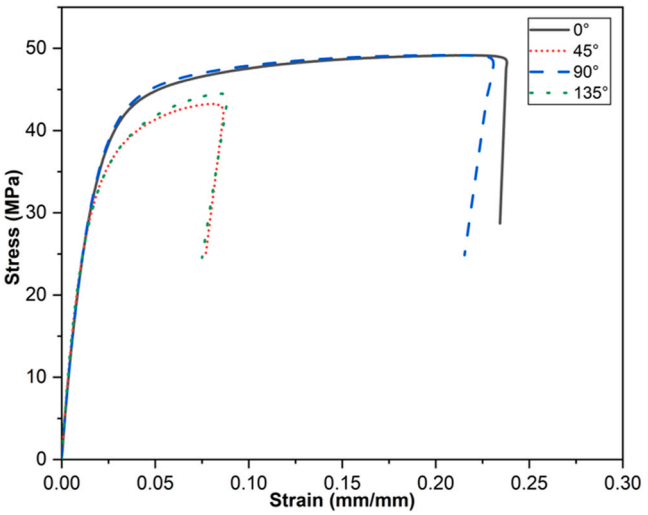

Fig. 6. Tensile test curves of specimens oriented at different angles on the printing platform.

3.2. Influence of positioning on mechanical properties

The results on part positioning are presented in Table 4. The Young's modulus of the XZ positioning is higher than that of XY and ZX. The difference between the XZ and XY Young's modulus is approximately 48%, indicating a significant difference between these two positioning

Table 4
Mechanical properties according to the positioning of the parts (average values and standard deviation).

	E_{mean}	Re_{mean}	Rm_{mean}
	(MPa)	(MPa)	(MPa)
XY	2437 ± 105	30 ± 3	48 ± 0.9
XZ	3608 ± 8	40 ± 1	60 ± 0.5
ZX	2341 ± 91	31 ± 1	31 ± 1

types. The XY Young's modulus is slightly higher than the ZX Young's modulus, with a difference of about 4%, suggesting a minor difference between these two positioning types. The analysis of other mechanical properties (yield strength and maximum strength) also shows similar trends.

A distinct difference in overall mechanical behavior is observed in the stress-strain curves presented in Fig. 7. The XY and XZ specimens exhibit ductile behavior compared to the ZX specimen, which displays brittle behavior indicative of inter-layer adhesion issues in Onyx. In their work, Marşavina et al. [7] also observed ductile and quasi-brittle fractures on specimens printed horizontally (XY) and vertically (XZ), respectively. Somireddy et al. [31] demonstrated that the printing direction significantly affects the mechanical behavior of printed parts. Similar observations were also made by Chacón et al. [5]. This confirms that 3D-printed parts exhibit anisotropic mechanical behavior depending on the printing direction.

The process anisotropy was determined using the anisotropy coefficient presented in Eq. 1. It was calculated by considering the yield strengths of the XY, XZ, and ZX specimens and the yield strength of the Onyx filament. The mechanical properties of the filament were evaluated previously. The Young's modulus ($E_{filament}$), yield strength ($Re_{filament}$), and maximum strength ($Rm_{filament}$) of the Onyx filament are 6809 $\pm$ 192, 56 $\pm$ 5.6, and 80 $\pm$ 9 MPa, respectively. The calculated coefficient is $I_{3D} = 30.71$, which is significantly higher than 0, indicating that the process induces a strong anisotropy in the mechanical properties of printed parts. Previous works, such as those by Ye et al. [25], on the mechanical-anisotropic properties of 3D-printed ultra-high ductility concrete, have shown an anisotropy coefficient ranging from 0.06 to 2.91. Dey et al. [26] showed that the anisotropy coefficient varies depending on the printing parameters and the manufacturing process.

3.3. Fracture analysis of samples

Fig. 8 displays the failure modes of the specimens after testing. Two main findings emerge: specimen failure occurs with the surface perpendicular to the tensile direction and with the surface inclined to the tensile direction. These observations were previously noted by Somireddy et al. [32] and Marşavina et al. [7] in their respective works.

The fracture surface of specimens oriented at 45° and 135° is perpendicular to the tensile direction. The reason for this behavior is that some layers of the specimens are parallel to the tensile direction (0° to the tensile direction), while others are perpendicular to it (90° to the tensile direction). At the mesoscopic scale, the printed layers behave like

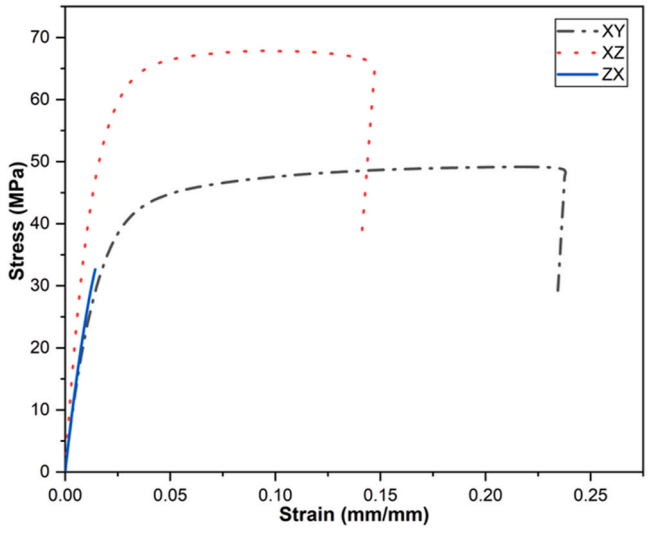

Fig. 7. Tensile test curves of samples according to the three positionings on the printing platform.

plies of composite materials. At 0° to the tensile direction, they are known to undergo brittle fracture. In addition, the failure of layers oriented at 90° is also brittle, as it characterizes the intra- and inter-layer adhesion.

Specimens with a fracture surface inclined to the tensile direction are those oriented at 0° and 90°. This is due to the shear stress state of the layers on a mesoscopic scale. Failure in such cases occurs progressively in the material along cracks. Based on the fracture modes of the specimens, it can be concluded that Onyx is an anisotropic material. This study did not consider failure modes.

3.4. Mechanical properties of walls and solid pattern

The mechanical properties of the walls and solid pattern were characterized for the XY and XZ specimens, as presented in Table 5.

The walls of the ZX specimen were not characterized due to limitations in the wall-cutting method, and scientifically, it has limited significance since the ZX positioning characterizes inter-layer adhesion. The stress-strain curves of the walls and solid pattern for both specimens are shown in Fig. 9.

The results revealed that the walls are stiffer and stronger than the solid patterns for the two studied positioning types. For the XY positioning, it was found that the walls are 70% stiffer and 55% stronger than the solid pattern. In the XZ positioning, the walls are 33% stiffer and 2% stronger than the solid pattern. Additionally, it was observed that the XY walls are stronger and stiffer than the XZ walls, in contrast to the XZ solid pattern, which is stronger and stiffer than the XY pattern. The tensile curves (Fig. 9) analysis demonstrated that the walls are less ductile than the solid patterns in both cases. The walls were 50% and 21% less ductile than the solid pattern for the XY and XZ positioning, respectively. The difference in mechanical behavior can be attributed to the lower porosity of the walls compared to the solid pattern (Section 3.6). This difference can also be explained by the number of layers in the XZ positioning, which is higher than in the XY positioning.

3.5. Wall influence on mechanical properties

The influence of the number of walls on the mechanical properties was also characterized, and the results are presented in Tables 6 and 7 for the three types of positioning.

These results showed that as the number of walls increases, the mechanical properties also increase for the XY and XZ positioning cases. In contrast, for the ZX positioning, the number of walls does not influence the mechanical properties. For example, between a 1-wall specimen and an 8-wall specimen (XY positioning), there is approximately a 54% and 50% difference in Young's modulus and yield strength, respectively. Similar observations were made for the XZ specimen. For the ZX specimen, there is an 8% difference in yield strength between the 1-wall specimen and the 3-wall specimen, with the difference remaining small.

The analysis of the overall behavior of the curves demonstrated that the ductility of the specimens decreases as the number of walls increases, as shown in Fig. 10. For instance, the 1-wall specimen is 56% more ductile than the 8-wall specimen. Liu et al. [8] showed that increasing the number of walls also improves the mechanical performance of 3D-printed parts, while Gebisa et al. [9] did not observe a significant influence of the number of walls on the mechanical properties.

3.6. Analysis of samples using X-ray tomography

X-ray tomography was employed to determine the porosity of the specimens and investigate whether there were differences in porosity based on the XY or XZ positioning. The tomographic analyses revealed porosity values of 2.1% for the walls, 8.4% for the XY specimens, and 1.13% for the ZX specimens. The tomographic images depicting the different porosities (walls, XY solid, and XZ solid) for the analyzed

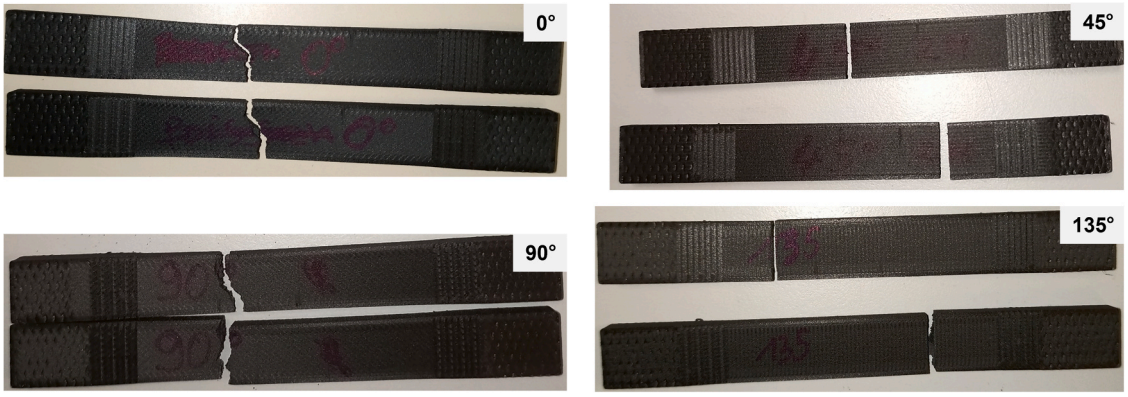

Fig. 8. Fracture of samples according to orientation.

Table 5
Mechanical properties of the walls and solid pattern of XY and XZ samples (average values and standard deviation).

	E_{mean}	Re_{mean}	Rm_{mean}
	(MPa)	(MPa)	(MPa)
XY Walls	5487 ± 114	53 ± 1.12	81 ± 3.2
XY Solid	1657 ± 149	24 ± 1.47	41 ± 1
XZ Walls	4340 ± 119	41 ± 1	64 ± 0.5
XZ Solid	2886 ± 97	40 ± 0.5	53 ± 1

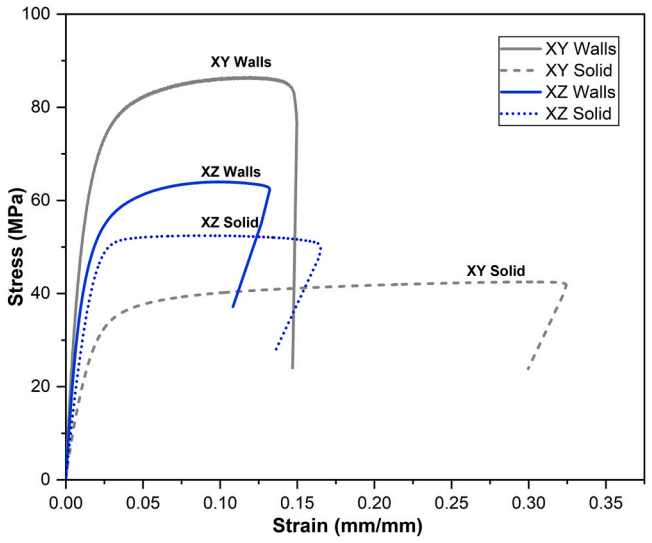

Fig. 9. Walls and solid tensile curves for XY and ZX positioning.

Table 6
Young's modulus (in MPa) of specimens according to the number of walls (average values and standard deviation).

	1 wall	2 walls	3 walls	4 walls	8 walls
	(MPa)	(MPa)	(MPa)	(MPa)	(MPa)
XY	1816 ± 52	2437 ± 105	-	2661 ± 50	3911 ± 59
XZ	3080 ± 46	3622 ± 40	4102 ± 74	-	-
ZX	2124 ± 30	2341 ± 92	2308 ± 171	-	-

elements are presented in Fig. 11 (a, b, and c). These images clearly demonstrate the varying porosity levels of the analyzed components.

Porosity values ranging from 8.3% to 9.2% were observed in work by Vidakis et al. [33], who used the same printing conditions but a different printer and material. Porosity is dependent on nozzle diameter, layer thickness, and layer deposition orientation, as shown by Delbart et al. [34] in their work, and they indicated that smaller nozzle diameters resulted in lower porosity percentages. These differences in porosity partially explain the variations in the mechanical properties of the walls, solid specimens, and XY and ZX specimens. Saeed et al. [35] and Mei et al. [36] demonstrated in their respective studies that reducing porosity can increase the mechanical properties of parts. It can be concluded that the porosity level of a 3D-printed part also impacts its mechanical properties.

Table 7
Yield stress (in MPa) of specimens according to the number of walls (average values and standard deviation).

	1 wall	2 walls	3 walls	4 walls	8 walls
	(MPa)	(MPa)	(MPa)	(MPa)	(MPa)
XY	22 ± 1.24	30 ± 3.2	-	30 ± 2.1	44 ± 0.5
XZ	37 ± 0.47	40 ± 0.43	46 ± 3.5	-	-
ZX	32 ± 0.5	30 ± 0.5	30 ± 2.49	-	-

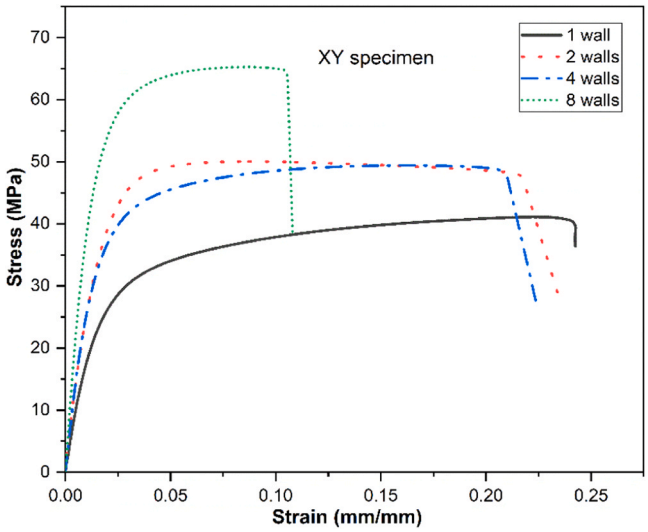

Fig. 10. Tensile stress curves of XY specimens according to the number of walls.

3.7. Analytical prediction of mechanical properties

Predicting mechanical properties is crucial, especially for this process involving multiple printing parameters. In this section, an approach based on the rule of mixtures (ROM) was implemented to predict these

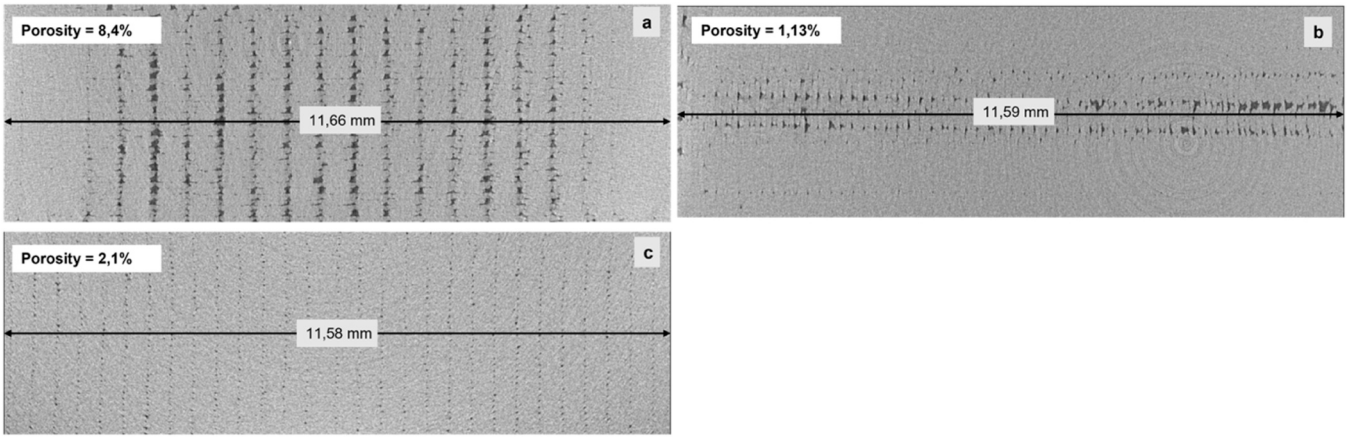

Fig. 11. X-ray tomographic image of (a) XY sample, (b) XZ sample, and (c) walls (XY and XZ).

mechanical properties (Young's modulus and yield strength) based on the number of walls and the positioning of the part on the printing bed. Fig. 12 depicts a simplified 2D model of a specimen that enabled the formulation of relations (Eq. 2) and (Eq. 3), based on the rule of mixtures, to predict Young's modulus and yield strength given the selected positioning type. The specimen was rectangular. It was assumed that the deformations at the surface of the specimen were equivalent to the deformations in the material volume. Additionally, it was assumed that the deformations of the layers (walls + solid infill) were identical: layers were 0.1 mm thick and could be modeled in 2D. The analytical model used to predict mechanical properties did not consider the presence of porosities in the specimens.

$$E = 0,8 * \frac{N_{walls}}{W} * \left(E(i)_{walls} - E(i)_{solid}\right) + E(i)_{solid} \quad (2)$$

$$\mathrm{Re} = 0,8 * \frac{N_{walls}}{W} * \left(\mathrm{Re}(i)_{walls} - \mathrm{Re}(i)_{solid}\right) + \mathrm{Re}(i)_{solid} \quad (3)$$

In these equations, N_{walls} represents the number of walls, and W represents the width of the part. Specifically, the width (W) is set to 12 mm for the XY positioning, while the XZ positioning is set to 4 mm. E refers to the Young's modulus, and Re represents the yield stress. The subscript (i) denotes the positioning, either XY or XZ.

The predicted results, experimental results, and prediction errors are presented in Table 8 and Table 9 for XY and XZ positioning. The prediction error is calculated using relation (Eq. 4). The results showed that the prediction model yields errors ranging from 0.6% to 12% and 5% to 15% for Young's modulus and yield strength, respectively (for the XY positioning). For the XZ positioning, the prediction error ranges from 3% to 9% and 1% to 13% for Young's modulus and yield strength, respectively.

$$Error \quad (\%) = 100 * \frac{Prediction - Experiment}{Prediction} \quad (4)$$

Table 8
Experiment vs. predicted Young's modulus and yield stress for XY positioning.

	$E_{Experiment}$	$E_{Predicted}$	Error	$Re_{Experiment}$	$Re_{Predicted}$	Error
	(MPa)	(MPa)	(%)	(MPa)	(MPa)	(%)
1 wall	1816	1912	5.03	22	26	15.16
2 walls	2437	2168	-12.42	30	28	-7.67
4 walls	2661	2678	0.64	30	32	5.46
8 walls	3911	3670	-5.71	44	39	-11.48

Table 9
Experiment vs. predicted Young's modulus and yield stress for XZ positioning.

	$E_{Experiment}$	$E_{Predicted}$	Error	$Re_{Experiment}$	$Re_{Predicted}$	Error
	(MPa)	(MPa)	(%)	(MPa)	(MPa)	(%)
1 wall	3080	3177	3.04	37	40	7.97
2 walls	3622	3468	-4.45	40	40	0.99
3 walls	4102	3758	-9.14	46	41	-13.3

The prediction errors generated by ROM are within acceptable ranges compared to other authors who use ROM for predicting the mechanical properties of long fiber composites. A study by Avanzini et al. [37] reported an error of 3% in their work on carbon fiber-reinforced onyx. However, Narajo-Lozada's [24] results showed a significant prediction error (up to 60%) when the volume fraction of fibers exceeds 11%. The present study shows that despite the high-volume fraction of the walls, the prediction errors do not exceed 15%. The observed errors in the reduced order model (ROM) can be attributed to the challenge of accurately estimating the ratio of walls and solid patterns. Furthermore, the lack of consideration for porosity in the calculations may also contribute to these variations. It may not be entirely accurate to assume that the deformations of the walls are identical to those of the pattern, which could also contribute to the

Fig. 12. Simplified model (2D) of a 3D-printed specimen.

deviations in prediction.

A GUI (Graphical User Interface) was developed using MATLAB App Designer (Fig. 13) to predict mechanical properties. It allows the user to input the sample's position, dimensions, and number of walls on the printing platform, thus obtaining the Young's modulus and yield strength as outputs.

4. Numerical modeling approaches

This section presents the numerical simulation models produced using the commercial finite element software Abaqus. The aim was to establish a numerical simulation methodology capable of considering both the positioning and the number of walls in printed parts. All simulations were carried out using the Abaqus CAE standard, using C3D8R solid elements without considering porosity effects. A convergence study was carried out for all models to eliminate the influence of element size (meshing) on the results, and the average element size retained was approximately 0.4 mm.

4.1. Numerical modeling of tensile tests

The objective of these simulations was to predict the behavior and mechanical properties of the specimens based on the number of walls. Table 10 provides the mechanical properties of the walls and solid pattern used in the simulation, including elasticity and plasticity parameters. The numerical model of the tensile test specimen is shown in Fig. 14, and the following steps are necessary to perform the simulation:

- The CAD model of the specimens was imported into Abaqus, and the walls of the solid fill were manually partitioned, assuming a perfect connection between the walls and the pattern. This ensures that the deformations in the tensile direction are identical, allowing for the generation of a continuous mesh at the interface between the walls and the pattern.
- The material properties corresponding to the walls and solid pattern were applied. The plastic behavior of the walls and pattern was identified using Hollomon's power law.
- The boundary and loading conditions applied were fixed boundary conditions and velocity load.
- A set of two nodes was created at 12.5 mm for the tensile test, corresponding to the extensometer's initial length. During the simulation, the displacements of both nodes and the reaction forces were recorded.
- Eqs. (5) and (6) were used to calculate the numerical strains (ε) and stresses (σ) based on the node displacements and reaction forces.

Table 10
Mechanical properties used in numerical simulation.

	Young's modulus (MPa)	Poisson's ratio	Hollomon plasticity parameters (K; n)
Walls (XY)	5412	0.3	135.5; 0.142
Solid (XY)	1660		63.62; 0.148
Walls (XZ)	2863		106.7; 0.141
Solid (XZ)	4340		97.51; 0.138

$$\boldsymbol{\varepsilon} = \frac{N_2 - N_1}{L_0} \tag{5}$$

$$\boldsymbol{\sigma} = \frac{Reaction \quad Forces}{A_0} \tag{6}$$

Where N_1 and N_2 represent the displacement of the set nodes and L_0 is the initial distance between the two nodes (12.5 mm). A_0 represents the initial cross-section of the sample (48 mm^2).

4.2. Numerical results of tensile tests

The initial simulations were conducted considering the number of walls in the test specimens and their positioning on the printing bed. Each simulation was carried out individually according to the procedure described in Section 4.1. The two main positioning configurations, XY and XZ, were considered with four and two walls, respectively. Fig. 15 (a and b) show the specimens' stress-strain curves and stress map, respectively.

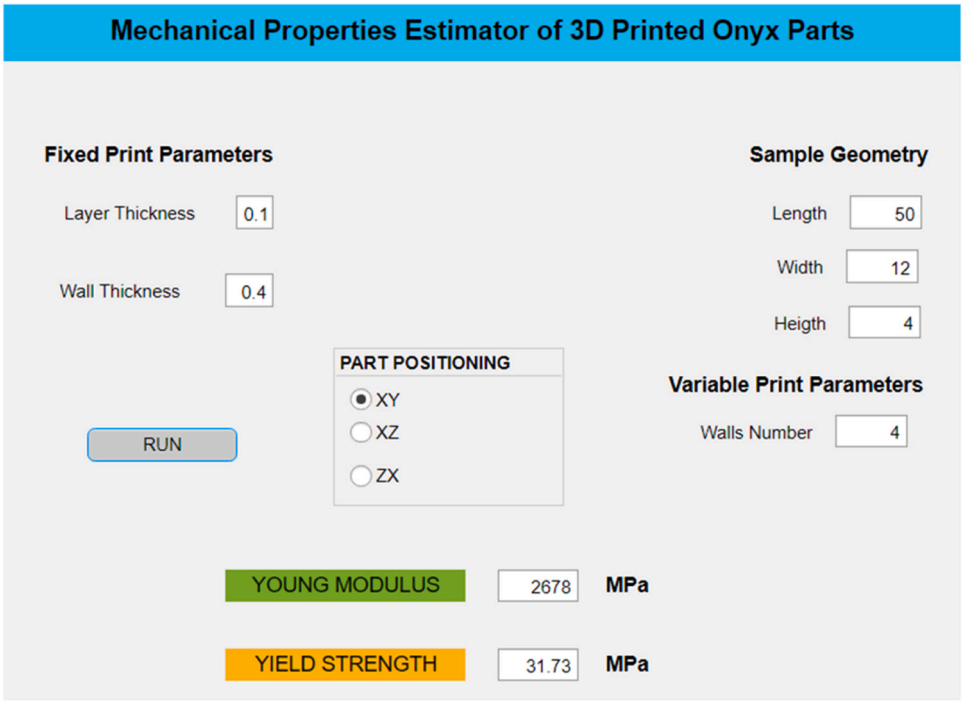

Fig. 13. GUI for mechanical properties prediction (developed in MATLAB R2018a).

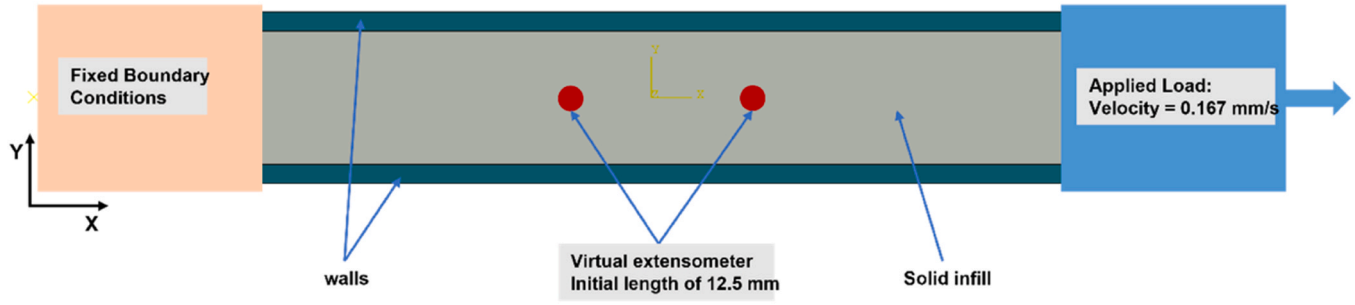

Fig. 14. Numerical tensile test setup.

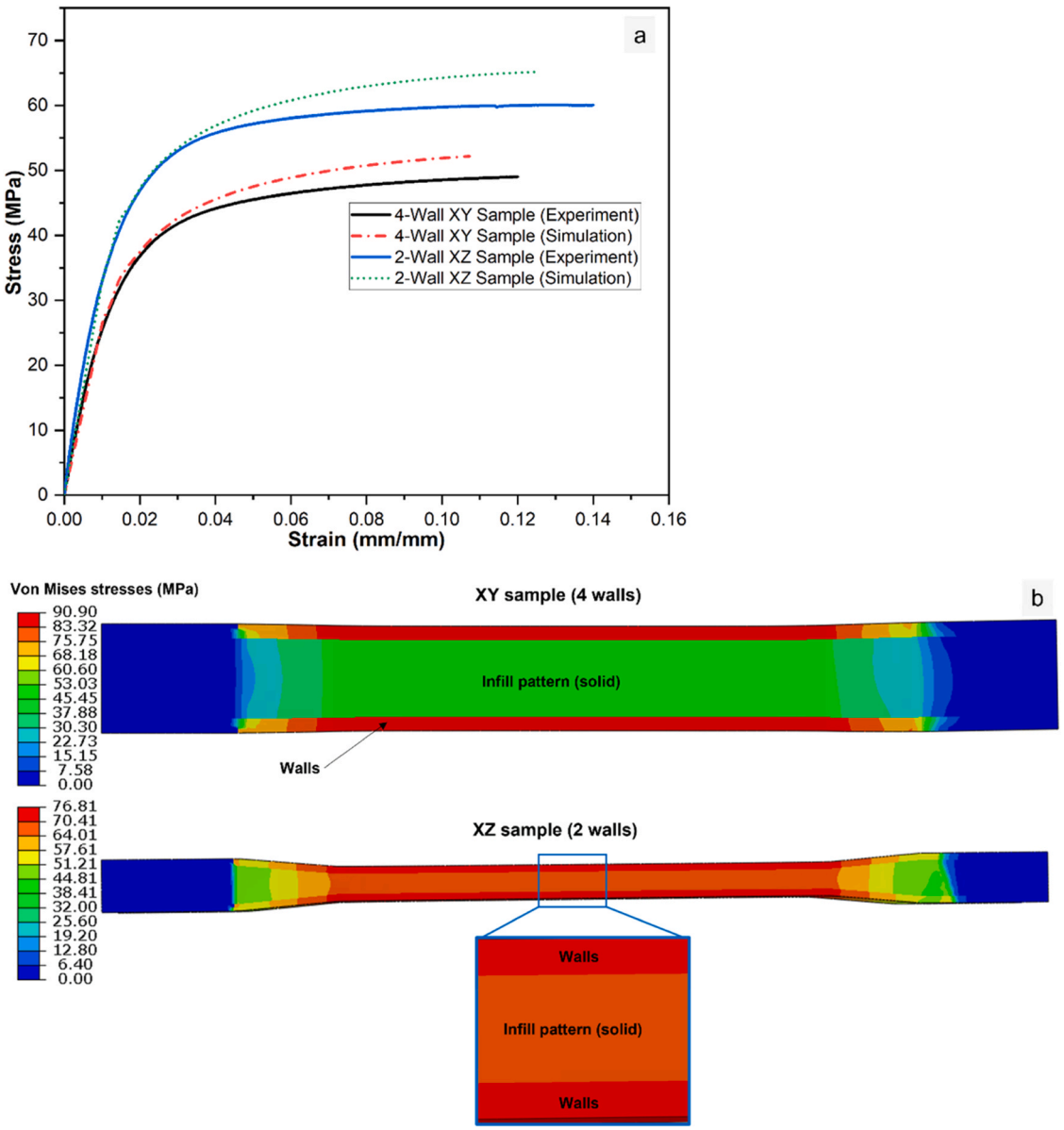

Fig. 15. Numerical simulation results of XY and XZ samples: (a) numerical vs experiment curves and (b) stress map.

The analysis of the stress fields reveals that the maximum stresses are always localized in the walls. The stress distribution is also symmetric in both specimens. The fundamental assumption for these simulations was continuity between the walls and the infill, and the connection between them was considered perfect.

The numerical curves (Fig. 15 (a) correlate well with the experimental curves in the elastic range and partially in the plastic range, too. However, for strains above 3%, the numerical curves no longer correlate with the experimental curves.

Table 11 presents the numerical results for Young's modulus and

Table 11
Comparison between experimental Young's modulus and numerical Young's modulus.

	$E_{Experiment}$	$E_{Simulation}$	Error	$Re_{Experiment}$	$Re_{Simulation}$	Error
	(MPa)	(MPa)	(%)	(MPa)	(MPa)	(%)
XY sample (4 walls)	2661	2630	-1.16	31	32	3.22
XZ sample (2 walls)	3622	3283	-9.35	40	43	7.5

yield strength of specimen XY (4 walls) and specimen XZ (2 walls), which are then compared with the experimental results.

The results demonstrate low prediction errors, between 1–10% and 3–8% for Young's modulus and yield strength, respectively, for both specimen types (XY and XZ). This validates the numerical simulation approach proposed in this study and justifies defining a separate specimen with different material properties for the walls and filling pattern.

This tool considers the impact of the number of walls on the elastic mechanical properties of 3D-printed parts. It can aid in dimensioning printed parts by determining the necessary number of walls to meet mechanical requirements before printing. The deviation between experimental and numerical results may be attributed to the absence of porosity considerations in numerical models or to the macroscopic scale of the modeling itself. A more precise prediction of mechanical properties could be achieved by modeling on a smaller scale that considers the differences in behavior between successive printed layers. One weakness of this study is that it does not consider failure modes in the numerical modeling. Although this may be useful for analyzing overall specimen behavior, it does not affect the prediction of elastic mechanical properties.

Simulation overestimates mechanical behavior. The most plausible explanation for the discrepancy between the numerical and experimental curves is the potential detachment between the walls and the infill during the tensile test, which was not accounted for in the simulation. One possible solution would be to use contact mechanics or cohesive elements between the walls and the infill. This would require characterizing the contact behavior between the walls and the infill to obtain their mechanical characteristics.

One of the main challenges in numerical simulation of 3D-printed parts arises when dealing with complex-shaped parts (e.g., as shown in Fig. 16 (a and b). In such cases, a single constitutive model may not be sufficient, and an alternative modeling approach is required to simulate these parts with as much accuracy as possible. A proposed simulation approach is discussed in the next section.

4.3. Numerical simulation approaches for complex geometry

When the printed part exhibits a complex shape, as depicted in Fig. 16 (a and b), the numerical simulation becomes intricate due to the involvement of two crucial parameters: positioning and number of walls, which are challenging to consider. To address this complexity, a simulation methodology was proposed in this study to achieve a high level of realism. The example part investigated in this work encompasses three positions (XY, XZ, and ZX) and three walls. This geometric shape was designed to have a section presenting the three identified positions (XY, XZ, and ZX). The dimensions were chosen to parameterize at least three walls in this part, which will be included in the numerical studies.

4.3.1. Methodology 1: Simulation with multiple isotropic models

An isotropic behavior model can be employed when dealing with less complex geometries and the possibility of wall segmentation. This involves segmenting the walls for each orientation and assigning the appropriate material parameters to each segment, as depicted in Fig. 17. The studied part was manually partitioned into five distinct zones (A to E), each representing the walls or the solid pattern based on the identified positioning. Zone A corresponds to the ZX positioning, where no differentiation is necessary between the walls and the solid pattern (as explained in Section 3.5). Using an isotropic behavior model, the simulation can capture the printed part's overall mechanical response, considering the walls' combined behavior and the solid pattern. It provides a practical solution to accurately predict the mechanical behavior and properties of the printed part, contributing to advancing additive

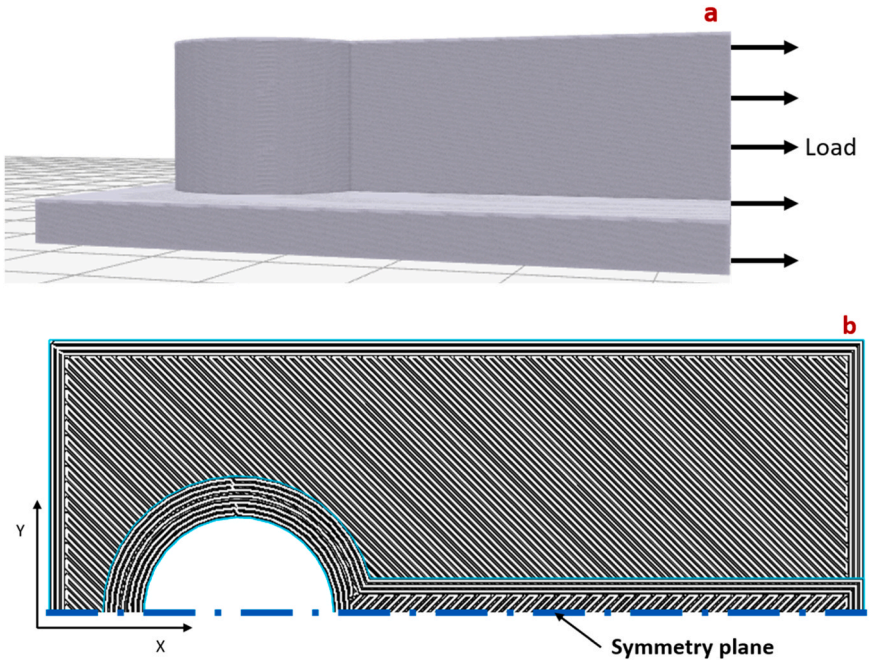

Fig. 16. Example part with three positionings. a: imported model in Eiger software and b: scaling of the part with three walls.

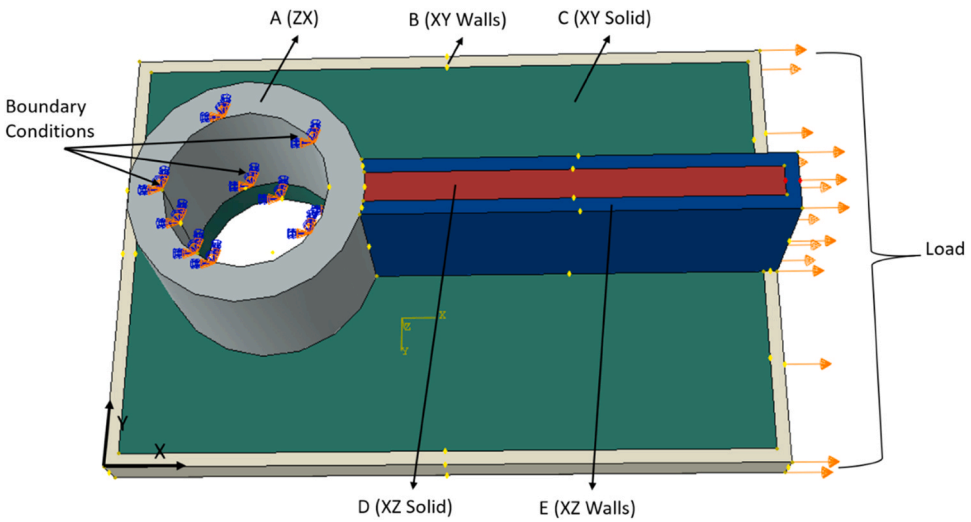

Fig. 17. Numerical model with isotropic material.

manufacturing techniques.

4.3.2. Methodology 2: Simulation with an orthotropic model

Simulation with a model becomes advantageous when wall segmentation is challenging due to complex geometries. In such cases, homogenization of the mechanical parameters for each positioning can be performed by considering the number of walls, as described by Eq. 2 in Section 3.4. By calculating the respective moduli, an orthotropic material model can be constructed (Eq. 5). To implement this model, the different parts corresponding to each positioning are partitioned, and local coordinate systems are created and applied accordingly. In the present example, three sections (A, B, and C) were identified, and their corresponding local coordinate systems were assigned. The resulting numerical model is illustrated in Fig. 18.

$$\begin{pmatrix} \varepsilon_{11} \\ \varepsilon_{22} \\ \varepsilon_{33} \\ \gamma_{12} \\ \gamma_{23} \\ \gamma_{13} \end{pmatrix} = \begin{pmatrix} 1/E_1 & -\upsilon/E_1 & -\upsilon/E_1 & 0 & 0 & 0 \\ -\upsilon/E_1 & 1/E_2 & -\upsilon/E_2 & 0 & 0 & 0 \\ -\upsilon/E_1 & -\upsilon/E_2 & 1/E_3 & 0 & 0 & 0 \\ 0 & 0 & 0 & 1/G_1 & 0 & 0 \\ 0 & 0 & 0 & 0 & 1/G_2 & 0 \\ 0 & 0 & 0 & 0 & 0 & 1/G_3 \end{pmatrix} \cdot \begin{pmatrix} \sigma_{11} \\ \sigma_{22} \\ \sigma_{33} \\ \tau_{12} \\ \tau_{23} \\ \tau_{13} \end{pmatrix} \tag{5}$$

With, $G_i = \frac{E_i}{2*(1+\upsilon)}$ (where i = 1 to 3, corresponding to the three positions of the parts).

The elastic constants of the orthotropic model for this part are: $E_1 = 3584$ MPa, $E_2 = 1892$ MPa, $E_3 = 2341$ MPa, $G_1 = 1347$ MPa, $G_2 = 711$ MPa, $G_3 = 900$ MPa et $\upsilon = 0.3$.

Considering the positioning and number of walls, this model allows for a more realistic representation of the mechanical response. Overall, this simulation methodology enables the accurate simulation of complex-shaped printed parts, incorporating the effects of positioning and the number of walls. It provides insights into the mechanical behavior and properties, contributing to the understanding and optimization of additive manufacturing processes.

4.3.3. Summary and comparison of numerical simulation approaches

The numerical simulation results using both behavior models are shown in Fig. 19 (a and b). The stress fields reveal that the maximum values are located in similar regions for both models. The orthotropic model can be an effective alternative for numerical simulation when using an isotropic model becomes challenging or even impossible. However, it is important to note that the orthotropic model does not account for plasticity, which may be necessary to capture the overall behavior of the printed part. To address this limitation, an orthotropic hardening model, such as the Hill model, can be incorporated into the simulation to capture the plastic behavior of the part. The advantage of

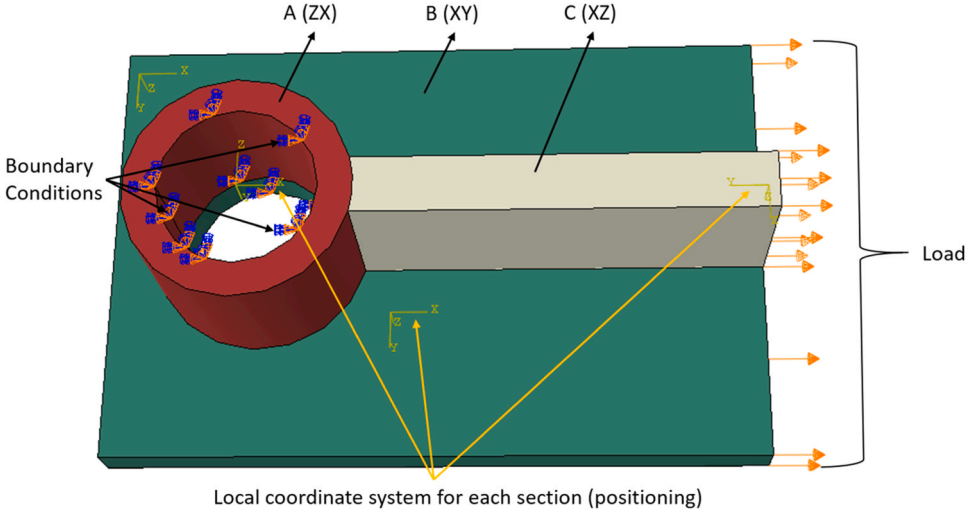

Fig. 18. Numerical model with orthotropic material.

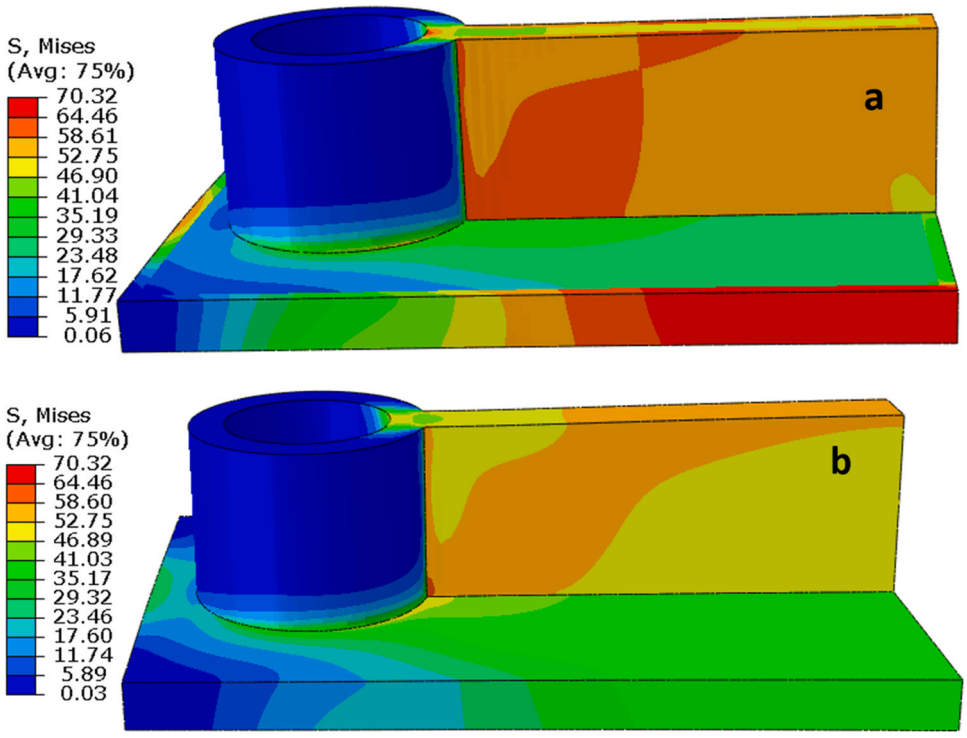

Fig. 19. Numerical simulation of the studied part: (a) isotropic model and (b) orthotropic model.

using isotropic models is that they allow for considering plasticity in each identified part, leading to more realistic results.

A comprehensive approach for simulating 3D-printed parts has been developed and presented in Fig. 20. It outlines the key steps in simulating printed parts while accounting for positioning and walls. This methodology provides a framework for accurately predicting the mechanical behavior and properties of 3D-printed parts, considering their specific geometries and manufacturing parameters. It enables engineers and researchers to optimize the design and manufacturing processes, leading to improved performance and reliability of 3D printed components.

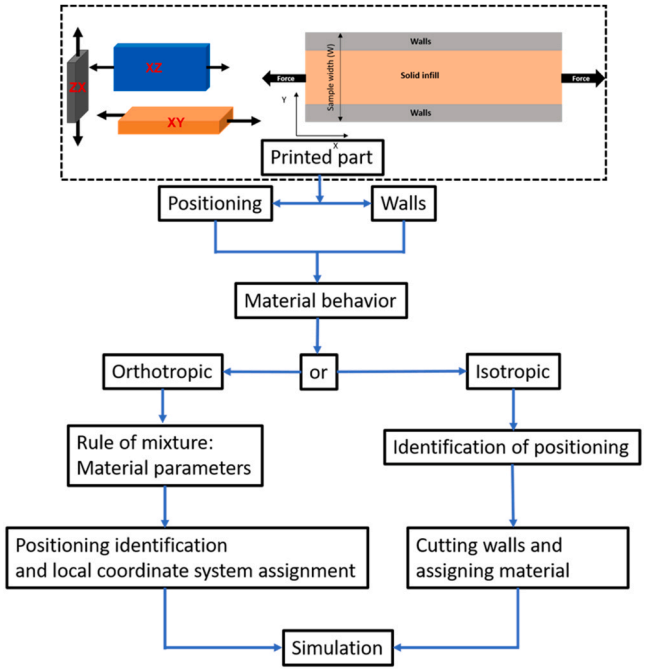

Fig. 20. Holistic workflow for the numerical simulation of 3D-printed parts.

5. Conclusion

This article investigated the mechanical properties of 3D-printed parts using Onyx material from various perspectives. The investigation focused on the influence of part orientation and positioning on the print bed, the effect of the number of walls, and the necessary steps for an efficient numerical simulation of printed parts. The main conclusions can be summarized as follows:

- The mechanical parameters of the printed parts are minimally affected by their orientation on the printing platform. The samples showed an average variation of ± 3.5% in Young's modulus.
- The mechanical properties of printed parts are significantly affected by their positioning on the printing platform. Samples oriented in the XZ direction were 48% stiffer than those oriented in the XY direction and 54% stiffer than those oriented in the ZX direction.
- In this study, wall effects were characterized, revealing an important impact on mechanical properties. Mechanical properties were improved by adding more walls.
- A rule of mixtures-based analytical model was proposed to predict the mechanical properties of specimens based on their positioning and number of walls. The observed prediction errors ranged from 1% to 15%.
- Numerical simulation approaches were proposed to consider the effect of walls and the positioning of the part. The observed prediction errors ranged from 1% to 9%. For parts with complex geometries, a global approach was proposed for numerical simulation that considers both part positioning and the number of walls.

In conclusion, this paper has investigated Onyx as an anisotropic material and the main printing parameters which were walls and positioning. In order to consider these parameters, analytical and numerical predictive models were developed. However, some limitations should be addressed in future work. Specifically, the non-inclusion of porosity and

the lack of consideration for the interaction between the walls and the solid pattern need improvement.

Ethical approval

This article contains no studies conducted by authors with human participants or animals.

Funding

This study was not funded by any funding source or organization.

CRediT authorship contribution statement

Daouda Nikiema: Conceptualization, Writing – review & editing; **Pascale Balland**: Resources, Project management, validation, Review & editing. **Alain Sergent**: validation, Writing, review & editing;.

Declaration of Competing Interest

The authors declare that they have no known competing financial interests or personal relationships that could have appeared to influence the work reported in this paper.

References

[1] T.T. Wohlers, I. Campbell, O. Diegel, R. Huff, J. Kowen, Wohlers Associates (Firm), Wohlers report 2022: 3D printing and additive manufacturing global state of the industry, n.d.
[2] Pahlevanzadeh F, Bakhsheshi-Rad HR, Brabazon D, Kharaziha M, Ismail AF, Sharif S, Razzaghi M, Berto F. Additive manufacturing of polymer matrix composites. Encycl Mater Compos 2021:1013–28. https://doi.org/10.1016/B978-0-12-819724-0.00025-2.
[3] Patel R, Desai C, Kushwah S, Mangrola MH. A review article on FDM process parameters in 3D printing for composite materials. Mater Today Proc 2022. https://doi.org/10.1016/j.matpr.2022.02.385.
[4] Prabhakar MM, Saravanan AK, Lenin AH, Leno IJ, Mayandi K, Ramalingam PS. A short review on 3D printing methods, process parameters and materials. Mater Today Proc 2020;45:6108–14. https://doi.org/10.1016/j.matpr.2020.10.225.
[5] Chacón JM, Caminero MA, García-Plaza E, Núñez PJ. Additive manufacturing of PLA structures using fused deposition modelling: effect of process parameters on mechanical properties and their optimal selection. Mater Des 2017;124:143–57. https://doi.org/10.1016/j.matdes.2017.03.065.
[6] Zou R, Xia Y, Liu S, Hu P, Hou W, Hu Q, Shan C. Isotropic and anisotropic elasticity and yielding of 3D printed material. Compos Part B Eng 2016;99:506–13. https://doi.org/10.1016/j.compositesb.2016.06.009.
[7] Marşavina L, Vălean C, Mărghitaş M, Linul E, Razavi N, Berto F, Brighenti R. Effect of the manufacturing parameters on the tensile and fracture properties of FDM 3D-printed PLA specimens. Eng Fract Mech 2022;274. https://doi.org/10.1016/j.engfracmech.2022.108766.
[8] Liu Y, Jiang W, Hu W, Ren L, Deng E, Wang Y, Song C, Feng Q. Compressive strength and energy absorption characteristics of the negative stiffness honeycomb cell structure. Mater Today Commun 2023;35:105498. https://doi.org/10.1016/j.mtcomm.2023.105498.
[9] Gebisa AW, Lemu HG. Influence of 3D printing FDM process parameters on tensile property of ultem 9085. Procedia Manuf, Elsevier B V 2019:331–8. https://doi.org/10.1016/j.promfg.2019.02.047.
[10] Gebisa AW, Lemu HG. Investigating Effects of Fused-Deposition Modeling (FDM) Processing Parameters on Flexural Properties of ULTEM 9085 using Designed Experiment 2018:1–23. https://doi.org/10.3390/ma11040500.
[11] Távara L, Madrigal C, Aranda MT, Justo J. Anisotropy and ageing effect on the mechanical behaviour of 3D-printed short carbon-fibre composite parts. Compos Struct 2023;321. https://doi.org/10.1016/j.compstruct.2023.117196.
[12] Khosravani MR, Anders D, Reinicke T. Effects of post-processing on the fracture behavior of surface-treated 3D-printed parts. CIRP J Manuf Sci Technol 2023;46:148–56. https://doi.org/10.1016/j.cirpj.2023.08.006.
[13] Nurizada A, Kirane K. Induced anisotropy in the fracturing behavior of 3D-printed parts analyzed by the size effect method. Eng Fract Mech 2020;239. https://doi.org/10.1016/j.engfracmech.2020.107304.
[14] Adibeig MR, Vakili-Tahami F, Saeimi-Sadigh MA. Numerical and experimental investigation on creep response of 3D printed Polylactic acid (PLA) samples. Part I: The effect of building direction and unidirectional raster orientation. J Mech Behav Biomed Mater 2023;145. https://doi.org/10.1016/j.jmbbm.2023.106025.
[15] Lupone F, Padovano E, Venezia C, Badini C. Experimental characterization and modeling of 3D printed continuous carbon fibers composites with different fiber orientation produced by FFF process. Polymers (Basel) 2022;14. https://doi.org/10.3390/polym14030426.
[16] Melenka GW, Cheung BKO, Schofield JS, Dawson MR, Carey JP. Evaluation and prediction of the tensile properties of continuous fiber-reinforced 3D printed structures. Compos Struct 2016;153:866–75. https://doi.org/10.1016/j.compstruct.2016.07.018.
[17] Chen AY, Baehr S, Turner A, Zhang Z, Gu GX. Carbon-fiber reinforced polymer composites: a comparison of manufacturing methods on mechanical properties. Int J Light Mater Manuf 2021;4:468–79. https://doi.org/10.1016/j.ijlmm.2021.04.001.
[18] Díaz-Rodríguez JG, Pertúz-Comas AD, González-Estrada OA. Mechanical properties for long fibre reinforced fused deposition manufactured composites. Compos Part B Eng 2021;211. https://doi.org/10.1016/j.compositesb.2021.108657.
[19] Pipalla R, Schuster J, Shaik YP. Experimental analysis on 3d printed onyx specimens with honeycomb infill structure. J Adv Mater Sci Eng 2021;1. https://doi.org/10.33425/2771-666x.1003.
[20] Domingo-Espin M, Puigoriol-Forcada JM, Garcia-Granada AA, Llumà J, Borros S, Reyes G. Mechanical property characterization and simulation of fused deposition modeling Polycarbonate parts. Mater Des 2015;83:670–7. https://doi.org/10.1016/j.matdes.2015.06.074.
[21] Khosravani MR, Rezaei S, Ruan H, Reinicke T. Fracture behavior of anisotropic 3D-printed parts: experiments and numerical simulations. J Mater Res Technol 2022;19:1260–70. https://doi.org/10.1016/j.jmrt.2022.05.068.
[22] Nikiema D, Balland P, Sergent A. Study of the mechanical properties of 3D-printed onyx parts: investigation on printing parameters and effect of humidity. Chin J Mech Eng Addit Manuf Front 2023;2:100075. https://doi.org/10.1016/j.cjmeam.2023.100075.
[23] Hasanov S, Gupta A, Nasirov A, Fidan I. Mechanical characterization of functionally graded materials produced by the fused filament fabrication process. J Manuf Process 2020;58:923–35. https://doi.org/10.1016/j.jmapro.2020.09.011.
[24] Naranjo-Lozada J, Ahuett-Garza H, Orta-Castañón P, Verbeeten WMH, Sáiz-González D. Tensile properties and failure behavior of chopped and continuous carbon fiber composites produced by additive manufacturing. Addit Manuf 2019;26:227–41. https://doi.org/10.1016/j.addma.2018.12.020.
[25] Ye J, Cui C, Yu J, Yu K, Dong F. Effect of polyethylene fiber content on workability and mechanical-anisotropic properties of 3D printed ultra-high ductile concrete. Constr Build Mater 2021;281. https://doi.org/10.1016/j.conbuildmat.2021.122586.
[26] Dey D, Sahu A, Prakash S, Panda B. A study into the effect of material deposition methods on hardened properties of 3D printed concrete. Mater Today Proc 2023. https://doi.org/10.1016/j.matpr.2023.03.034.
[27] Žmindák M, Novák P, Soukup J, Milosavljevic D, Kaco M. Finite element simulation of tensile test of composite materials manufactured by 3D printing. IOP Conf Ser Mater Sci Eng 2020;776. https://doi.org/10.1088/1757-899X/776/1/012082.
[28] Kalova M, Rusnakova S, Krzikalla D, Mesicek J, Tomasek R, Podeprelova A, Rosicky J, Pagac M. 3d printed hollow off-axis profiles based on carbon fiber-reinforced polymers: Mechanical testing and finite element method analysis. Polymers (Basel) 2021;13. https://doi.org/10.3390/polym13172949.
[29] Benamira M, Benhassine N, Ayad A, Dekhane A. Investigation of printing parameters effects on mechanical and failure properties of 3D printed PLA. Eng Fail Anal 2023;148. https://doi.org/10.1016/j.engfailanal.2023.107218.
[30] Sága M, Bárnik F, Vaško M, Handrik M, Kopas P. Identification of physical characteristic of composite materials produced by additive technology from perspective of selected mechanical properties. Acta Physica Polonic 2020;138:249–52. https://doi.org/10.12693/APhysPolA.138.249.
[31] Somireddy M, Czekanski A. Anisotropic material behavior of 3D printed composite structures – material extrusion additive manufacturing. Mater Des 2020;195. https://doi.org/10.1016/j.matdes.2020.108953.
[32] Somireddy M, Singh CV, Czekanski A. Mechanical behaviour of 3D printed composite parts with short carbon fiber reinforcements. Eng Fail Anal 2020;107. https://doi.org/10.1016/j.engfailanal.2019.104232.
[33] Vidakis N, David C, Petousis M, Sagris D, Mountakis N. Optimization of key quality indicators in material extrusion 3D printing of acrylonitrile butadiene styrene: The impact of critical process control parameters on the surface roughness, dimensional accuracy, and porosity. Mater Today Commun 2023;34. https://doi.org/10.1016/j.mtcomm.2022.105171.
[34] Delbart R, Papasavvas A, Robert C, Quynh Truong Hoang T, Martinez-Hergueta F. An experimental and numerical study of the mechanical response of 3D printed PLA/CB polymers. Compos Struct 2023:117156. https://doi.org/10.1016/j.compstruct.2023.117156.
[35] Saeed K, McIlhagger A, Harkin-Jones E, McGarrigle C, Dixon D, Ali Shar M, McMillan A, Archer E. Characterization of continuous carbon fibre reinforced 3D printed polymer composites with varying fibre volume fractions. Compos Struct 2022;282. https://doi.org/10.1016/j.compstruct.2021.115033.
[36] Mei H, Ali Z, Yan Y, Ali I, Cheng L. Influence of mixed isotropic fiber angles and hot press on the mechanical properties of 3D printed composites. Addit Manuf 2019;27:150–8. https://doi.org/10.1016/j.addma.2019.03.008.
[37] Avanzini A, Battini D, Giorleo L. Finite element modelling of 3D printed continuous carbon fiber composites: Embedded elements technique and experimental validation. Compos Struct 2022;292. https://doi.org/10.1016/j.compstruct.2022.115631.